

A novel technique for optimization of BLDC-based dual-motor electric vehicles using adaptive BFO-based PID controller

Rajnish Kumar, Amitesh Kumar

Nextgen Adaptive Systems Group, Department of Electrical Engineering, National Institute of Technology Patna, Bihar, India

Article Info

Article history:

Received Jan 18, 2024

Revised Oct 15, 2024

Accepted Oct 23, 2024

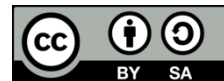
Keywords:

Adaptive BFO
BLDC motor
Dual motor
Electric scooter
PID control

ABSTRACT

This study addresses the imperative for electric vehicle (EV) propulsion systems to operate at higher speeds with effective motor control, given the rapid advancement of EV technology. Specifically focusing on electric 2-wheelers, we aim to enhance their maximum speed range from 45 km/hr to 110 km/hr by optimizing the control strategy of a widely used commercial e-bike from Vespa. Our approach explores the feasibility of employing a dual motor system instead of a single motor, coupled with optimization techniques for a proportional-integral-derivative (PID) controller governing a linear brushless DC (BLDC) motor. Implemented in MATLAB/Simulink, our method offers advantages such as consistent convergence, ease of implementation, and high computational efficiency. By employing bacterial foraging optimization (BFO) along with an adaptive BFO (ABFO) technique to optimize the PID controller, we achieve significantly faster response times compared to conventional BFO methods. These findings underscore the efficacy of our approach in enhancing the speed control and acceleration characteristics of EV propulsion systems, contributing to the ongoing evolution of electric mobility solutions.

This is an open access article under the [CC BY-SA](#) license.



Corresponding Author:

Amitesh Kumar

Nextgen Adaptive Systems Group, Department of Electrical Engineering

National Institute of Technology Patna

Patna, Bihar 800005, India

Email: amitesh.ee@nitp.ac.in

1. INTRODUCTION

Electric vehicles (EVs) are essential for advancing transportation infrastructure, replacing internal combustion engines (ICE) to reduce fossil fuel use. Growing demand stems from recent technological advancements, making EVs a sustainable alternative to traditional vehicles [1], [2]. According to the Society of Indian Automobile Manufacturers or SIAM, India is the world's largest producer and two-wheeler market, with about 20 million sold annually, comprising over 80% of the nation's vehicle market [3]. Electrifying two-wheelers can significantly reduce emissions, but progress is slow due to battery inefficiencies, limited energy storage, high costs, restricted speed and range, and challenges in selecting suitable electric motors [1], [4]. EVs use a variety of motor types, like DC motors [5], induction motors (IM) [6], permanent magnet synchronous motors (PMSM) [7], switched reluctance motors (SRM) [8], brushless DC (BLDC) motors (BLDCM) [9], [10]. In commercial EVs, IM and BLDCM are commonly used. IM is the most affordable and durable but has drawbacks like low power factor and poor efficiency [11]. In contrast, BLDC provides several benefits over IM, including greater power factor, good dynamic responsiveness, low noise, and higher efficiency because there is no rotor winding, and it is of compact size due to a high torque torque-to-weight ratio [4]. For EVs

BLDC motors are promising but are costly due to the required converter and controller. However, precise motor control can make them more affordable [12], [13].

Over recent decades, industrial process control systems have evolved significantly, with strategies like fuzzy control [13], and neural control [14], adaptive control [15], [16] offering more efficient, flexible, and intelligent solutions for complex industrial operations. The proportional-integral-derivative (PID) controller is popular in the industry for its simplicity and robustness, but its high order makes tuning challenging. Adjusting controlling parameters K_p , K_i , K_d are essential to fulfill the performance requirements like steady-state error, steady-state time, and overshoot [17]. So, the parameter selection is the key to the PID controller design because it directly affects the system's control performance. The initial approach for setting PID controller design relies upon Z-N method [18]. In many areas of industrial control, it is difficult to find optimal value using Z-N method. Since then, many researchers have focused on intelligent algorithms such as fuzzy control [13] and neural control [14], but these algorithms require a high control process. Hence, an evolutionary algorithms like artificial bee colony (ABC) [19] optimization, particle swarm optimization (PSO) [17], ant colony optimization (ACO) [20], and bacterial foraging optimization (BFO) are used for self-tuned PID controller parameters.

Evolutionary algorithms like PSO, ABC, ACO, and the bat algorithm are preferred over conventional techniques like hill climbing [21], perturb and observe [22] and incremental conductance [23] due to their effectiveness in handling multi-modal optimization problems in parameter extraction. Genetic algorithms (GA) have drawbacks like slow convergence and poor performance with complex fitness functions. Particle swarm optimization (PSO) addresses these issues for parameter extraction [24], [25]. This method yields better PID constants but increases iterations, leading to longer computation time and poor local search ability. Multiple optima can cause premature convergence, which can degrade the performance. However, with the use of BFO has several advantages. It is based on natural selection, which excludes solutions using ineffective foraging techniques. It eliminates premature convergence and its convergence speed is faster than PSO [26]. BFO is more accurate than PSO and widely used to design PID controller constants. However, its fixed step size may prevent finding the true optimal point [27]. This problem is solved by taking variable step size for that an adaptive model is discussed in this paper. No work has been reported on implementing BFO to control EVs' electric drive. Electric scooters and light vehicles need good transient behavior for quick acceleration, while heavy vehicles prioritize steady-state behavior for constant-speed operation [28].

The analysis focuses on comparing dual motors with single motors in EVs. In a chassis-mounted configuration, the motor connects to rear wheel of the shaft via a transmission system with fixed gear ratios, typically ranging from 1:6 to 1:10 [29], [30], depending on motor specifications and the required vehicle torque and speed. In-wheel motors offer improved size and efficiency compared to traditional mounted motors, which are typically designed for low torque and high speed. However, the system's overall efficiency declines due to the series coupling of the motor, transmission, and rear wheel [31]. To compensate for this efficiency loss and achieve greater range, a larger battery is required [32]. Additionally, electric scooters with single motors face limitations in speed range due to transmission losses. This limitation can be mitigated by employing dual motors, which enhance performance and extend the operational range by reducing the impact of transmission inefficiencies [33], [34].

A dual motor method is discussed in this paper which helps 2-wheeler EV in achieving higher speed with respect to 2-wheeler EVs with a single motor. The existing electric scooter available in the market for commercial use is equipped with a single motor, which is replaced by one additional electric motor (EM) with a power rating for higher speed operation, improving the overall speed and efficiency. Furthermore, a widely used electric scooter, Vespa Elettrica, is utilized by the prestigious company Vespa to improve the speed range for validation. This paper is structured in five sections. Section 1 is the introduction part. Section 2 focuses on vehicle modeling, outlining the forces exerted on the scooter. In section 3, the mathematical model, transfer function (TF), and PID controller for the BLDCM are discussed. Section 4 details the process of determining the PID controller constants and introduces an adaptive BFO method. Section 5 covers BLDCM's dynamic equations and provides an analysis of a dual motor setup. The final section presents the results and analysis.

2. ELECTRIC VEHICLE MODELLING

The dynamics of EVs are generally categorized into motor dynamics and vehicle dynamics. The two are connected through a transmission system that includes a gearing mechanism. Important factors in vehicle dynamics modeling include acceleration, aerodynamic resistance, and road conditions. The vehicle model in Figure 1 illustrates the forces applied to the electric scooter. The motor provides a tractive effort (TE) to drive the electric scooter forward. This TE is countered by aerodynamic drag (F_{ad}) from air resistance, rolling resistance (F_{rr}) due to friction, and hill-climbing force (F_{hc}) from the road's incline. The TE can be expressed by F_{te} and given as in (1). To achieve acceleration, the TE must overcome these opposing forces. The expressions for these forces are given in (2).

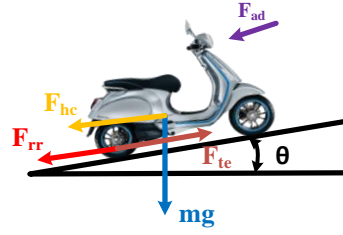


Figure 1. Forces applied on the electric scooter [35]

Thus, the TE can be expressed by F_{te} and given as in (1):

$$F_{te} = F_{rr} + F_{hc} + F_{ad} + F_{la} + F_{\omega a} \quad (1)$$

where F_{la} represents force due to linear acceleration and $F_{\omega a}$ denotes force due to angular acceleration.

$$F_{te} = \mu_{rr} mg \cos \theta + mg \sin \theta + 0.5 * \rho A C_d v^2 + ma + I \frac{G^2}{\eta_g r^2} a \quad (2)$$

Where ' μ_{rr} ' represents rolling resistance, ' g ' is acceleration due to gravity, ' m ' represents average mass, ' ρ ' represents air density, ' A ' is scooter frontal area, ' C_d ' represents drag co-efficient, ' I ' represents rotor's moment of inertia, ' v ' is the vehicle velocity, ' G ' is the gear ratio, ' η_g ' is efficiency of gear system and ' r ' is the wheel's radius.

Since angular acceleration of any vehicle is significantly lesser than the linear acceleration. So, it can often be disregarded, accounting for only about 5% of the value of linear acceleration. This simplification results in an effective 5% increase in the total mass to account for angular effects [13].

3. BRUSHLESS DC MOTOR

EM is vital in an EV's drive system. A BLDCM is a variant of permanent magnet (PM) synchronous motors, distinguished by the waveform of its induced electromagnetic field (EMF). When the EMF waveform is sinusoidal, it is classified as a PMSM. And if waveform of induced EMF is trapezoidal, then it is called as PM brushless DC motor (PMBLDC) [36]. DC motors are popular in EVs for their strong speed-torque characteristics, but issues with brushes and the commutator require frequent maintenance, making them less suitable. Brushless DC motors overcome this issue by eliminating brushes while maintaining similar torque-speed characteristics, offering improved reliability and reduced maintenance, making them a better choice for electric vehicles [37]. This is why the BLDCM is widely used in EVs and HEVs applications. It provides various benefits such as a compact design, low weight relative to output power (high power density), increased efficiency, quiet performance, extended lifespan, wide speed range, and effective heat dissipation. These benefits make it ideal for modern electric and hybrid vehicle systems [38], [39].

DC motors utilize mechanical rectifiers and brushes for commutation, while BLDCMs depend on hall effect sensors. In a BLDCM, the coils are located in the stator, and the rotor consists of PMs. The rotor's movement is driven by the magnetic fields produced by the stator, with hall effect sensors used to detect its position. Since BLDCMs use PM instead of armature coils, they eliminate the need for brushes, improving efficiency and reducing maintenance [40].

This section focuses on the mathematical model and control approach for the BLDCM in an electric scooter. Figure 2 presents the control strategy, which utilizes a PID controller optimized through BFO and ABFO algorithms. The PID controller operates in series with the motor. The TF of the BLDCM is derived using speed as both the input and the output. A speed command serves as the reference for the desired output, with the output characteristics discussed in section 4.

3.1. Mathematical modelling

The voltage equations governing the behavior of the BLDC motor can be formulated as in (3). Since back EMF of the electric motor is directly linked to its speed, so, it is given by (4). The equations for the load torque and electromagnetic torque of the BLDCM are given by (5) and (6).

$$V_i(t) = L * \frac{di(t)}{dt} + e_b(t) + R * i(t) \quad (3)$$

$$e_b(t) = K_b \omega(t) \quad (4)$$

$$T(t) = J \frac{d\omega(t)}{dt} + B\omega(t) \quad (5)$$

$$T(t) = K_t i(t) \quad (6)$$

Where $V_i(t)$ voltage applied on the motor, $i(t)$ is the motor's stator current, $e_b(t)$ is motor's back EMF, $\omega(t)$ is the motor speed, L and R are the inductance and stator resistance, respectively, B is the viscous coefficient, T is the motor torque, J is moment of inertia, K_t and K_b are electromagnetic torque and back constant respectively. The motor's parameters are listed in Table 1, are used to determine the motor's TF.

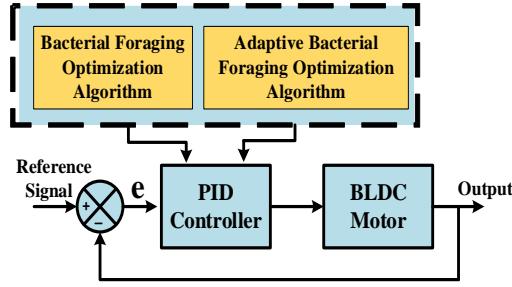


Figure 2. A block diagram of BLDCM integrated with a PID controller

Table 1. BLDC motor specifications taken in this research work

Sl No.	Parameters	Rating
a.	Rated voltage	24 V
b.	Rated current	8.5 A
c.	Rated Speed (Ns)	2300 rpm
d.	Rated Power	200 W
e.	Inductance per phase	40 μ H
f.	Resistance per phase (R)	27.739 m Ω
g.	Torque Constant (k_t)	0.087248 Nm/A
h.	Back-emf constant (K_b)	9.133 V/krpm
i.	Rotor inertia (J)	0.0031095 Nms ²

3.2. Transfer function

To derive the motor's TF, the Laplace transform (LT) is applied to the equations. The resulting equations, after performing the LT, are as in (7)-(11).

$$V_i(S) = LS * I(S) + E_b(S) + R * I(S) \quad (7)$$

$$E_b(S) = K_b * \omega(S) \quad (8)$$

$$T(S) = K_t * I(S) \quad (9)$$

$$T(S) = B * \omega(S) + JS * \omega(S) \quad (10)$$

By equating (9) and (10), $I(S)$ can be found out as:

$$I(S) = \left(\frac{B+JS}{K_t} \right) * \omega(S) \quad (11)$$

Substitute $E_b(S)$ and $I(S)$ from (8) and (11) in (7), $V_i(S)$ can be obtained as:

$$V_i(S) = \frac{((SL + R)*(JS + B) + K_t * K_b) * \omega(s)}{K_t}$$

Thus, the TF of the BLDCM is expressed as in (12).

$$\frac{\omega(S)}{V_i(S)} = \frac{K_t}{LJS^2 + (R*J + L*B)S + (R*B + K_t*K_b)} \quad (12)$$

3.3. PID controller

PID control is mostly used in industrial applications because of its simplicity. It is robust and reliable and also it has ease of tuning. It combines three control actions which are proportional (P), integral (I), and derivative (D). A proportional controller decreases system error in proportion to its gain but cannot completely eliminate it. To resolve this, an integral controller is added, which minimizes the steady-state error to almost zero and enhances the system's response time. The derivative controller, on the other hand, minimizes system overshoot, though it tends to increase response time. Together, these elements make the PID controller highly effective for precision control [41]. The PID controller block diagram is represented in Figure 3. Effective tuning of the PID controller enhances motor performance [42]. To achieve optimal tuning, an adaptive BFO algorithm is introduced, offering improved response characteristics compared to the classical BFO method. This approach is further detailed in section IV. The dynamical expression in the S-domain for the output of the above controller is expressed as is (13).

$$U(S) = K_p E(S) + \frac{K_I}{S} E(S) + K_D S \quad (13)$$

The controller output in the time domain is expressed as in (14).

$$e(t) = K_p e(t) + K_I \int e(t)dt + K_D \frac{de(t)}{dt} \quad (14)$$

Where K_P = It represents a gain of a proportional controller; K_I = It represents a gain of an integral controller; and K_D = It represents a gain of a derivative controller.

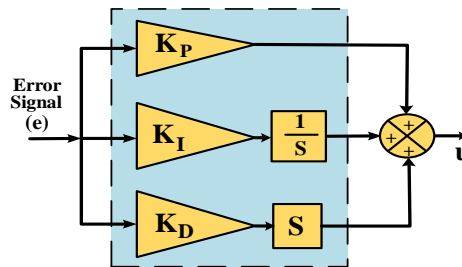


Figure 3. PID controller

4. OPTIMIZATION TECHNIQUES

The PID controller constants for BLDCM can be adjusted by using different optimization techniques. This study presents a new approach, ABFO, and compares its performance to the traditional BFO method for enhanced results. Optimization entails finding a solution for a problem by either minimizing or maximizing a specific objective function within a specified range while adhering to given constraints. Several solutions may satisfy these requirements and optimize the objective function, and these are called acceptable solutions. The best of these is known as the optimal solution. BFO techniques have been used to determine controller parameters, and their results are compared with those obtained using the adaptive BFO algorithm, which aims to provide a more efficient and effective solution to the problem.

4.1. Bacterial foraging optimization (BFO)

The BFO algorithm is a stochastic search method which is introduced by Passino in 2002 [43] and it is inspired by a foraging behavior of bacteria called *Escherichia coli*, typically found in the human intestines. BFO is termed a social foraging algorithm because bacteria within a colony cooperate during the search and foraging process. For this collective strategy to succeed, each bacterium must be able to move and respond to environmental inputs. Additionally, bacteria must share information so that the colony can benefit from each other's successes. The core functions of BFO reflect these principles of social foraging, as outlined below [26], [44]. Figure 4 illustrates the flowchart of the BFO process. Whereas, a block diagram is shown in Figures 5 and 6 which uses BFO and ABFO respectively to find the optimized value of the PID controller parameter.

a. Initialization

Random locations representing the controller's parameters and target structures are generated for each bacterium in the colony. In this step, various key parameters are initialized, including the following:

n – number of dimensions in search space

S – the total count of bacteria within the population

N_s – swimming length

N_c – total count of chemotactic steps

N_{re} – total count of reproduction steps

P_{ed} – the probability of elimination-dispersal (E-D)

N_{ed} – the count of E-D events

$C(i)$ – the step size in a randomly chosen direction is defined by the tumble action

b. Chemotaxis

In traditional BFO, a "tumble" denotes a single step in a random direction, while a "run" signifies a step continued in the direction of the previous move. Let $\theta^i(j, k, l)$ denote the positions of i^{th} bacterium during the j^{th} chemotactic, k^{th} reproductive and l^{th} E-D step. The step size for each run or tumble is denoted by $C(i)$. During chemotaxis, the motion for the i -th bacterium is represented as in (15):

$$\theta^i(j+1, k, l) = \theta^i(j, k, l) + C(i) \frac{\Delta(i)}{\sqrt{\Delta^T(i)\Delta(i)}} \quad (15)$$

where $\Delta(i)$ is a vector in a random direction whose value present between $[-1, 1]$. At each stage of this process, a run or tumble activity is performed, and step fitness, designated as $J(i, j, k, l)$ is assessed.

c. Swarming

This function simulates the dynamics of attraction and repulsion among cells. It describes how bacteria release attractants to congregate in areas with high nutrient levels while foraging in regions with decreasing nutrients. To prevent the colony from diverging to low-nutrient areas, it also stimulates the production of repellents by bacteria feeding in those regions.

d. Reproduction

This function occurs after the bacterial colony has completed the required number of chemotaxis steps. The starting phase of BFO reproduction consists of assessing each bacterium's fitness. In the subsequent phase, half of the colony, comprising the least fit bacteria, is removed. The top-performing bacteria are duplicated, with each surviving bacterium creating two copies, supporting the ongoing development of the colony.

e. Elimination and dispersal (ED)

The algorithm incorporates dispersion events to adjust the colony's behavior, ultimately providing the optimal controller parameters upon completion.

f. Termination

After completing a specified number of ED events, the procedure concludes. The method then returns the optimal controller parameters as its final output.

4.1.1. Bacterial foraging optimization algorithm (BFOA)

The classical BFOA follows these steps to determine an optimal solution for the objective function:

- Step 1 – Initialize the parameters $n, S, N_s, N_c, N_{ed}, N_{re}, P_{ed}, C(i), i = 1, 2, 3, \dots, S$
- Step 2 – E-D process: $l = l + 1$
- Step 3 – Reproduction cycle, $k = k + 1$
- Step 4 – Chemotactic cycle, $j = j + 1$
 - a. For $i = 1, 2, 3, \dots, S$ Perform a chemotaxis step for the i -th bacterium as follows –
 - b. Calculate the fitness function $J(i, j, k, l)$
 - c. Let $J_{\text{last}} = J(i, j, k, l)$ to retain this value, as a better cost may be discovered during a run
 - d. Tumble: It will generate a random vector $\Delta(i) \in \mathbb{R}^p$ where each element in $\Delta_m(i)$, $m = 1, 2, 3, \dots, p$ is a randomly generated number with in the range $[-1, 1]$.
 - e. Move: Let

$$\theta^i(j+1, k, l) = \theta^i(j, k, l) + C(i) \frac{\Delta(i)}{\sqrt{\Delta^T(i)\Delta(i)}}$$

- f. Calculate $J(i, j+1, k, l) = J(i, j, k, l) + J_{cc}(\theta^i(j+1, k, l), P(j+1, l))$.
- g. Set the swim length to, $m = 0$. This loop will continue till it met the condition $m = N_s$. otherwise, it will continue. If $J(i, j, k, l) < J_{\text{last}}$ (indicating an improvement), then replace $J_{\text{last}} = J(i, j+1, k, l)$ and let the equation be written as -

$\theta^i(j+1, k, l) = \theta^i(j, k, l) + C(i) \frac{\Delta(i)}{\sqrt{\Delta^T(i)\Delta(i)}}$ and substitute value of $\theta^i(j+1, j, k)$ to calculate the value of $J(i, j+1, k, l)$.

- h. Proceed to subsequent bacterium ($i+1$) if $i \neq S$ (i.e., move to 'b' to process the subsequent bacterium).
- Step 5 – If $j < N_c$, move on to step 4 and continue the chemotactic process as long as the bacterium's life cycle is not yet complete.
- Step 6 – Reproduction: For the specified reproduction (k) and E-D (l) and for each bacteria i.e $i=1, 2, 3, \dots, S$, let (16) represents the health of i^{th} bacterium.

$$J_{health}^i = \sum_{j=1}^{N_c+1} J(i, j, k, l) \quad (16)$$

The initial top S_r bacteria with the highest J_{health} values will perish. Meanwhile, the remaining S_r bacteria with the best performance will undergo reproduction.

- Step 7 – if $k < N_{re}$, return to step 3. If the specified number of reproduction steps has not yet been achieved, initiate the next generation of the chemotactic loop.
- Step 8 – Elimination-dispersal (E-D): The ED probability P_{ed} , determines the likelihood of eliminating and dispersing each bacterium, maintaining a constant total population size. If $l < N_{ed}$, return to step 2 otherwise, conclude the process. These steps are also illustrated in the flowchart presented in Figure 4.

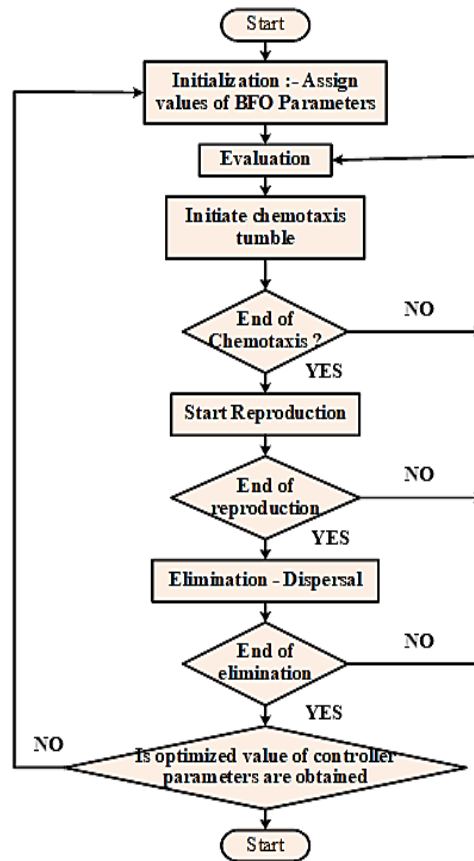


Figure 4. Flow diagram of the BFO technique

4.1.2. Result and analysis

The BFO algorithm is used to optimize PID controller, and that is used to control the BLDCM as shown in Figure 4. In this PID control, a step command of speed is applied as a reference signal and the corresponding output is obtained, as shown in Figure 7. In the response, the rise time is about 14 μsec , while its settling time is approximately 26 μsec . It is clearly seen from the response curve that there is no overshoot and undershoot in the system. Hence, the transient response is very good, enabling the motor to start quickly,

which supports fast acceleration of the vehicle when BLDC is used in electric vehicle. At steady-state conditions also the response characteristics is very good, and the error is only 0.4% in this condition. Table 2 shows the motor's step response parameters with optimized controller constants derived using the BFO technique.

4.2. Adaptive BFO technique (ABFO)

In the classical method of BFO technique, the chemotaxis step is the core of the BFO technique. The run-length step size is a crucial factor in the chemotaxis process, as it influences both the diversity and convergence of the population. The step size in the classical BFO technique is fixed, which suffers two main problems. First is, if the step size $C(i)$ is very less then bacteria will require too many steps to reach an optimum point. So, bacteria will be concentrated in a small part of the search space. Hence, the rate of convergence will decrease, and challenging to reach global optimum point. Second is, if step size $C(i)$ is very large then the bacteria will move fast to the optimized value but the result precision is low which causes bacteria to fall near local optima.

The differential-based optimization and precise control over local and global exploration is quite difficult to find an optimum solution. This adaptive BFO technique mainly focuses on finding the global optimum with a variable step size $C(i)$. The convergence speed is improved self-adaptive step size shown in the (17):

$$C(i)_{new} = C(i) * \left(1 - e^{\frac{-J^i(X)}{J^i(X) + \varepsilon}} \right) \quad (17)$$

where $J^i(X)$ is the i -th bacteria fitness function value and ' ε ' is an arbitrary constant. The sensitivity of chemotaxis step is improved with step size use in the (17). In the vicinity of the local or global optima the optimum point obtained by fixed step size may not reach the actual optima. The step size needs to be changed to get actual optima. The (17) decides step size of chemotaxis step. This equation improves further the cost of objective function. So, in ABFO, the chemotaxis step is modified to find the step size. The proposed chemotaxis loop of the ABFO algorithm is as follows:

4.2.1. Chemotaxis loop

In the optimization process, each bacterium undergoes a series of chemotactic steps to explore the solution space. For $i = 1, 2, 3, \dots, S$ starts by evaluating the fitness function $J(i, j, k, l)$, and set $J_{last} = J(i, j, k, l)$. This value is stored as a reference, allowing the algorithm to track improvements in subsequent iterations. Following this, a tumbling step is performed by generating a random vector $\Delta(i) \in R_p$ where each element $\Delta_m(i)$, for $m = 1, 2, 3, \dots, p$, is a randomly generated number within the range $[-1, 1]$. Let the equation given below produce a step size of $C(i)$ in the tumble direction for the bacterium i .

$$\theta^i(j+1, k, l) = \theta^i(j, k, l) + C(i) \frac{\Delta(i)}{\sqrt{\Delta^T(i) \Delta(i)}}$$

Calculate the value of $J(i, j+1, k, l) = J(i, j, k, l) + Jcc(\theta^i(j+1, k, l), P(j+1, k, l))$. Initialize swim length, i.e $m = 0$. This will continue till it met the condition $m = N_s$. Otherwise, it will continue. If $J(i, j, k, l) < J_{last}$ then replace $J_{last} = J(i, j+1, k, l)$ and let the equation given below use $\theta^i(j+1, j, k)$ to calculate the new $J(i, j+1, k, l)$.

$$\theta^i(j+1, k, l) = \theta^i(j, k, l) + C(i) \frac{\Delta(i)}{\sqrt{\Delta^T(i) \Delta(i)}}$$

Now, update step size with the given equation - $C(i)_{new} = C(i) * \left(1 - e^{\frac{-J^i(X)}{J^i(X) + \varepsilon}} \right)$ and proceed towards next bacterium $(i+1)$ if $i \neq S$ (that is, navigate to 'b' to handle subsequent bacterium).

4.2.2. Result and analysis

The value of PID controller constants is determined using the ATLBO technique, as illustrated in the Figure 6. The response characteristics of BLDCM are depicted in Figure 7. The performance characteristics obtained from the ABFO technique for BLDCM has better response compared to the response obtained from the BFO technique. In the overall response of the BLDCM, rise time is around 5 μ sec, the settling time is around 9 μ sec, and there is no overshoot and undershoot present in the system. Hence, the transient response is very good, which enables the motor to start and stop quickly. Hence, this characteristic supports quick acceleration and deceleration when used in electric vehicles. The response characteristics are also very good at

steady state conditions because its steady state error is only 0.15%. Table 2 depicts parameters having different characteristics of the motor's step response with optimized value of controller constants derived by the ABFO algorithm. A comparative response is shown in Figure 7, which shows that ABFO has a better response than the BFO technique.

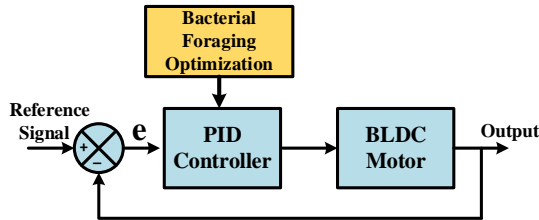


Figure 5. Optimal PID control using the BFO algorithm

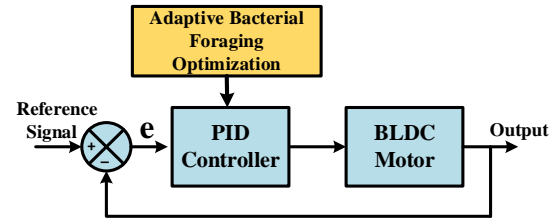


Figure 6. Optimal PID control using the ABFO algorithm

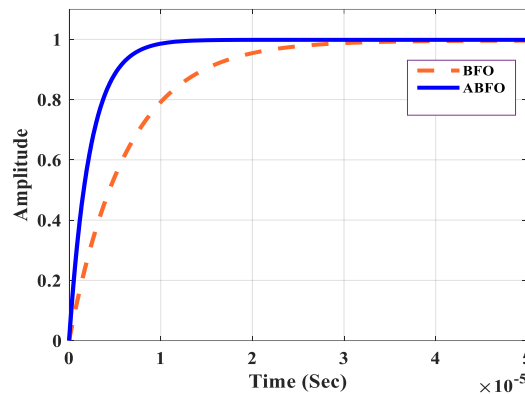


Figure 7. Response characteristics of BFO and ABFO

4.3. Comparative analysis

The results achieved for the BLDCM in this study have been compared and analyzed alongside several studies from the existing literature. Table 2 shows the comparative analysis. Jigang *et al.* [41] optimized a PI controller for speed control using a modified differential evolution algorithm, achieving a 2.47% maximum overshoot, with rise and settling times of 14 ms and 31 ms, respectively, under instantaneous change of load. Likewise, Ibrahim *et al.* [45] used a GA to perform optimal PID control of BLDCM. In this study, a PID controller is used, employing the integral absolute error (IAE) and integral square error criteria. The response characteristics are based on the IAE criterion which are presented in a comparison table, with a rise time of 51.1 μ s and a settling time of 91.1 μ s. Kommula and Kota [17] used a modified firefly-based PSO algorithm to optimize a fractional order PID controller for controlling a BLDCM. Their results, as listed in the comparison table, are for a motor speed of 2000 rpm and torque of 1.5 Nm [17]. In this literature, the results show a peak overshoot of 0.7% and a settling time of 0.254 seconds. Wang *et al.* [15], Shuraiji and Shneen [46] explored fuzzy PID and adaptive fuzzy PID controllers for BLDCM control. Wang *et al.* [15] reported a peak time and settling time of 40 ms at a speed of 2997 rpm, with a steady-state error of 2.9 rpm. Shuraiji and Shneen [46] reported a rise time of 19.53 ms, a peak in overshoot is 1.531%, and an undershoot is 11.924% for their fuzzy PID controller.

The comparative study of the works shows that the results obtained using ABFO in this research are more optimized. Among the reviewed literature, the lowest reported overshoot is 0.7%, while ABFO achieves zero overshoot. Likewise, the shortest settling time in prior research is 40 ms, but ABFO drastically reduces it to 9.155 μ s. This analysis highlights that ABFO offers superior optimization of the controller constants, resulting in a faster response time for vehicle acceleration. Thus, ABFO proves to be a more efficient approach for achieving optimal controller performance in electric vehicle systems.

Table 2. Comparative analysis of BFO, ABFO, and another optimization algorithm

Algorithm	Rise time	Settling time	Peak time	Peak overshoot	Peak undershoot	Peak	Steady-state error	Ref.
BFO	14.088 μ sec	26.009 μ sec	67.159 μ sec	0	0	0.996	0.004	This work
ABFO	5.076 μ sec	9.155 μ sec	24.221 μ sec	0	0	0.9985	0.0015	This work
Adaptive fuzzy PID	~	40 ms	40 ms	~	~	~	2.9 rpm	[15]
Modified firefly based PSO	~	0.254 sec	~	0.7 %	~	~	~	[17]
Differential evolution-based PI	0.014 sec	0.031 sec	~	2.47 %	~	~	0	[41]
GA based PID	51.1 μ sec	91.1 μ sec	~	0	~	1	0	[45]
Fuzzy PID	19.53 ms	~	~	1.531 %	1.788 %	~	~	[46]

5. DYNAMICS OF AN ELECTRIC BIKE

This particular section examines the dynamics of an electric scooter, with an emphasis on the BLDCM utilized in this research. Additionally, the Vespa Elettrica e-bike is evaluated using experimental data from the BLDCM installed in that specific scooter. In Table 3, the first part presents the parameters for the BLDCM from this study, while the second part includes the motor specifications for the Vespa Elettrica. To improve the performance of the Vespa Elettrica e-bike, a dual-motor configuration is proposed. A corresponding study has been conducted to assess the potential benefits of this setup, including improved speed, torque, and overall efficiency, contributing to enhanced vehicle dynamics.

Table 3. Motor parameters for electric scooter design

Sl no	Parameters	Our motor	Motor utilized in the Vespa Elettrica electric scooter
1.	Motor type	BLDC	BLDC
2.	Motor Power	200 W	4 KW (max)
3.	Maximum speed	110 km/h	45 km/h
4.	Diameter of wheel	30.48 cm (Front) 27.94 cm (rear)	30.48 cm (Front) 27.94 cm (rear)
5.	Mass of scooter	130 kg	130 kg
6.	Average mass of passenger	65 kg	65 kg
7.	Frontal area	0.7 m ²	0.7 m ²
8.	Drag co-efficient	0.5	0.5
9.	Gear ration	4.48:1	4.48:1
10.	Rolling resistance (μ_r)	0.007	0.007

5.1. Analysis of forces acting on the BLDC motor used in this study

The TE generated by EM can be determined by using (2). By substituting the BLDCM parameters listed in Table 3, the resulting TE is calculated as in (18). To examine the velocity characteristics of the motor over time, two scenarios are evaluated: startup and running. During startup, the motor requires maximum torque, which decreases as the motor transitions to running mode. The torque needed at startup is higher, while it reduces with increasing speed once the motor is operational. The maximum torque generated by EM can be found as in (19) and (20).

$$F_{te} = 13.40 + 0.2044 v^2 + 204.75 \frac{dv}{dt} \quad (18)$$

$$\text{Since the back emf is, } E = K_m \varphi * \left(\frac{2\pi N}{60} \right) \quad (19)$$

$$\text{i.e, } K_m * \varphi = \left(\frac{60}{2\pi} \right) * \frac{E}{N}, \quad (20)$$

Hence, the maximum torque at startup is expressed as in (21).

$$T_m = K_m \varphi I_{max} \quad (21)$$

Since the current can reach up to 4-5 times the maximum rated value for a few seconds, we use $I_{max} = 40.0$ A at startup. Consequently, the maximum torque T_m is 4 N-m. The TE can be calculated using the (22).

$$F_{te} = \frac{G}{r} \eta_g T_m = 125.712 \quad (22)$$

Therefore, (18) is expressed as in (23).

$$125.712 = 13.40 + 0.2044v^2 + 204.75 \frac{dv}{dt}$$

$$\text{As a result, } \frac{dv}{dt} = 0.5485 - 0.0009982 v^2 \quad (23)$$

In the running condition of the scooter, it can be seen in (24).

$$T = \frac{K_m \phi * E}{R_a} - \frac{(K_m \phi)^2}{R_a} * \omega \quad (24)$$

$$T = 86.254 - 2.565v$$

Substitute T in place of Tm in (22) to determine the vehicle's tractive effort, resulting in (18) as in (25).

$$\frac{dv}{dt} = 13.174 - 0.393v - 0.000998v^2 \quad (25)$$

After solving (23) and (25) the velocity versus time characteristics are obtained and it is shown in Figure 8. The BLDCM exhibits a starting torque of 4.0 N-m. The torque remains constant initially for up to 17 seconds, then decreases inversely with speed to maintain constant motor power. When the speed approaches approximately 40 km/h, then the torque continues to decrease because the speed is rising, ultimately stabilizing at around 0.95 N-m at peak speed. This torque is consistent during steady-state operation. Figure 9 presents the torque characteristics of the BLDCM.

5.1.1. Result analysis

Speed versus time characteristics of the BLDCM are shown in Figure 8, showing that the motor struggles with initial acceleration due to insufficient torque, requiring approximately 20 seconds to reach 40 km/h. However, after this initial period, the motor accelerates rapidly, reaching about 110 km/h within a few seconds. At a steady state, it maintains a top speed of 110 km/h. This indicates that while the motor is not well-suited for starting the vehicle, it performs effectively under running conditions. Therefore, based on these speed-time characteristics, the motor is well-suited for electric scooters. In the following section, the Vespa Elettrica electric bike is analyzed to determine its speed-time characteristics. Additionally, a solution to enhance its maximum speed is proposed by adding a second motor. The torque-speed response and control strategy for the dual-motor setup have been discussed earlier.

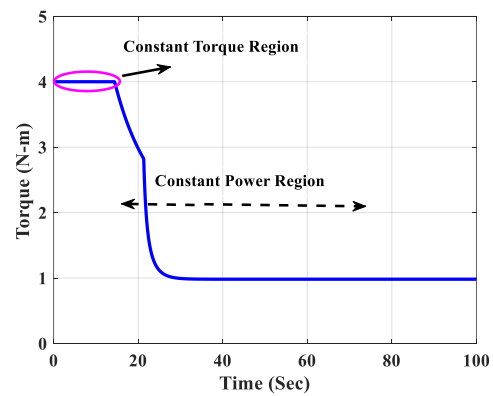
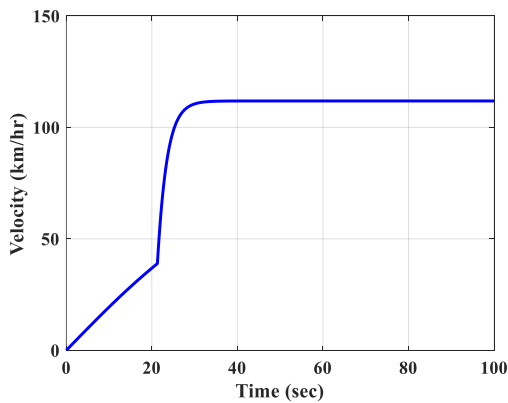


Figure 8. Speed-time characteristics of the BLDCM Figure 9. Torque characteristics of the BLDCM

5.2. Force analysis for the BLDCM utilized in the 'Vespa Elettrica' electric scooter

The TE is determined using (2). By applying the motor parameters for the Vespa Elettrica, as shown in Table 3, the total TE is determined as in (26).

$$F_{te} = 13.40 + 0.2044 * v^2 + 204.75 * \frac{dv}{dt} \quad (26)$$

To determine the speed-time characteristics of the motors, two scenarios must be considered: first, during the initial startup, and second, while the vehicle is in motion. During startup, the motor needs to deliver maximum torque, which can be calculated similarly to the method used for the first motor.

$$T_m = K_m \varphi * I_{max}$$

At the instant of startup, the current reaches maximum because in this instant back emf is not present. Therefore, the maximum starting current can be calculated by dividing the voltage by the armature resistance, which gives a maximum 83.33A current. Substituting this value of I_{max} into the torque equation gives a maximum torque of 44.7 newton-meter. Consequently, the TE is determined in (27) which is the corresponding value based on maximum torque.

$$F_{te} = \frac{G}{r} * \eta_g * T_m = 1404.80 \quad (27)$$

Therefore, the rate of change of velocity found in (28).

$$627.144 = 13.4 + 0.2044v^2 + 204.75 \frac{dv}{dt}$$

$$\text{Thus, } \frac{dv}{dt} = 6.79 - 0.000998v^2 \quad (28)$$

In the running condition of the motor, it adheres to (24). Hence, the value can be determined as:

$$T = 44.70 - 3.56v$$

By substituting 'T' into (27), the TE of the vehicle can be calculated. As a result, (26) is in (29). By solving (28) and (29) with MATLAB, the speed versus time characteristics is obtained, as shown in Figure 10.

$$\frac{dv}{dt} = 6.79 - 0.546v - 0.000998v^2 \quad (29)$$

5.2.1. Result analysis

The dynamics characteristics of speed versus time of the Vespa Elettrica electric scooter are shown in Figure 10, indicating strong initial acceleration, allowing it to reach 45 km/h within just three seconds. However, its maximum speed is also 45 km/h, as stated in the scooter's specifications [35]. While this makes it ideal for urban commuting, it means the scooter cannot exceed this speed limit, resulting in a constrained speed range. Overall, the scooter is well-suited for city travel but lacks the capability for higher-speed performance.

For light vehicles like electric scooters, rapid acceleration and deceleration are essential, necessitating an effective transient response. The transient responses of both motors are illustrated in Figure 8 and Figure 10. The additional motor used in Vespa Elettrica electric scooter demonstrates superior transient dynamic characteristics in terms of speed versus time. By employing both motors, the speed range can exceed 45 km/h. This dual-motor setup successfully meets both requirements: providing a strong transient response for rapid initial acceleration while attaining a greater maximum speed. The dynamic characteristics of dual motor configuration are presented in Figure 11.

The discussed dynamical characteristics demonstrate that the Vespa Elettrica electric scooter achieves rapid acceleration; however, to reach higher speeds, it must transition to a different motor. This switch enables an increase in overall speed, as the motor designed for high-speed operation requires less torque. Consequently, the current demand decreases, leading to reduced losses in the motor. This efficiency allows for better energy conservation from the battery, ultimately extending the vehicle's range on a single charge.

In this dual-motor setup, the motor responsible for high initial torque is mounted on the rear wheel, optimizing acceleration from a standstill. In contrast, the motor designed for speeds exceeding 45 km/h is located on the front wheel, where high torque is unnecessary for sustained performance. Together, these motors facilitate a top speed of 110 km/h. It is essential to recognize that the aforementioned analysis assumes a zero-degree incline. If the scooter encounters an incline, additional hill-climbing force will be required to maintain performance and ensure safe operation, which must be considered in practical scenarios.

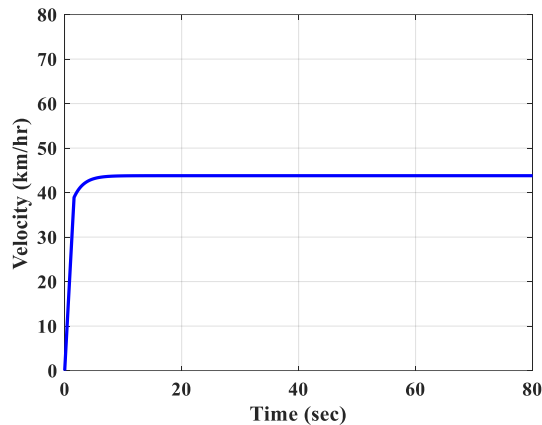


Figure 10. Speed vs. time characteristics of the BLDCM

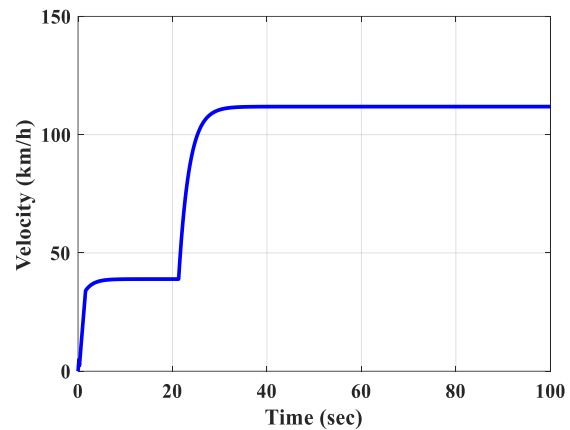


Figure 11. Speed vs. time characteristics of dual motor

6. CONCLUSION

The BLDCM, equipped with a PID controller, is optimized using both classical and adaptive BFO algorithms for electric vehicle applications, making it ideal for high-speed performance in electric scooters. The optimization using adaptive BFO is found to be significantly better than the classical approach of BFO. Additionally, the results are compared with existing literature, demonstrating that the proposed scheme significantly outperforms previous methods and can advance EV technology. Employing two motors with different power ratings enhances the overall speed range of the system, providing better performance. A higher-rated motor drives the rear wheel for enhanced starting torque, while a lower-rated motor at the front wheel boosts speed after initial acceleration. This dual-motor setup increases the Vespa Elettrica e-bike's speed range from its 45 km/hr to 110 km/hr and extends its range per battery charge, optimized using ABFO for superior transient response over traditional BFO methods. This research holds promising potential to greatly improve the performance of modern two-wheeled electric vehicles.

ACKNOWLEDGEMENT

The authors thank the Department of Science and Technology (DST), Government of India, for financial support via the DST SERB Project (File No. SRG/2021/002110). Dr. Amitesh Kumar acknowledges DST SERB for a Start-up Research Grant at NIT Patna, and Mr. Rajnish Kumar thanks the Ministry of Education and NIT Patna for providing the research facilities.

REFERENCES





- [1] A. Emadi, Y. J. Lee, and K. Rajashekara, "Power electronics and motor drives in electric, hybrid electric, and plug-in hybrid electric vehicles," *IEEE Transactions on Industrial Electronics*, vol. 55, no. 6, pp. 2237–2245, 2008, doi: 10.1109/TIE.2008.922768.
- [2] M. S. Munsif and H. Chaoui, "Energy Management Systems for Electric Vehicles: A Comprehensive Review of Technologies and Trends," *IEEE Access*, vol. 12, no. February, pp. 60385–60403, 2024, doi: 10.1109/ACCESS.2024.3371483.
- [3] Society of Indian Automobile Manufacturers, "Automotive Domestic Sales Trend." [Online]. Available: <https://www.siam.in/statistics.aspx?mpgid=8&pgidtrail=14>
- [4] P. H. Kumar and V. T. Somasekhar, "An Enhanced Fault-Tolerant and Auto-Reconfigurable BLDC Motor Drive for Electric Vehicle Applications," *IEEE Journal of Emerging and Selected Topics in Industrial Electronics*, vol. 4, no. 1, pp. 1–13, 2022, doi: 10.1109/jestie.2022.3196818.
- [5] Q. Zhang, J. Deng, and N. Fu, "Minimum Copper Loss Direct Torque Control of Brushless DC Motor Drive in Electric and Hybrid Electric Vehicles," *IEEE Access*, vol. 7, pp. 113264–113271, 2019, doi: 10.1109/ACCESS.2019.2927416.
- [6] J. Mei, Y. Zuo, C. H. T. Lee, and J. L. Kirtley, "Modeling and Optimizing Method for Axial Flux Induction Motor of Electric Vehicles," *IEEE Transactions on Vehicular Technology*, vol. 69, no. 11, pp. 12822–12831, 2020, doi: 10.1109/TVT.2020.3030280.
- [7] J. Lara, J. Xu, and A. Chandra, "Effects of Rotor Position Error in the Performance of Field-Oriented-Controlled PMSM Drives for Electric Vehicle Traction Applications," *IEEE Transactions on Industrial Electronics*, vol. 63, no. 8, pp. 4738–4751, 2016, doi: 10.1109/TIE.2016.2549983.
- [8] K. Diao, X. Sun, G. Lei, Y. Guo, and J. Zhu, "Multimode Optimization of Switched Reluctance Machines in Hybrid Electric Vehicles," *IEEE Transactions on Energy Conversion*, vol. 36, no. 3, pp. 2217–2226, 2021, doi: 10.1109/TEC.2020.3046721.
- [9] A. Dadashnialehi, A. Bab-Hadiashar, Z. Cao, and R. Hoseinnezhad, "Reliable EMF-Sensor-Fusion-Based Antilock Braking System for BLDC Motor In-Wheel Electric Vehicles," *IEEE Sensors Letters*, vol. 1, no. 3, pp. 1–4, 2017, doi: 10.1109/lsens.2017.2705087.
- [10] F. Mahmouditabar, A. Vahedi, and N. Takorabet, "Robust Design of BLDC Motor Considering Driving Cycle," *IEEE Transactions on Transportation Electrification*, vol. 10, no. 1, pp. 1414–1424, 2024, doi: 10.1109/TTE.2023.3285650.

- [11] P. Mishra, A. Banerjee, and M. Ghosh, "FPGA-Based Real-Time Implementation of Quadral-Duty Digital-PWM-Controlled Permanent Magnet BLDC Drive," *IEEE/ASME Transactions on Mechatronics*, vol. 25, no. 3, pp. 1456–1467, 2020, doi: 10.1109/TMECH.2020.2977859.
- [12] A. Eldho Aliasand and F. T. Josh, "Selection of Motor foran Electric Vehicle: A Review," *Materials Today: Proceedings*, vol. 24, pp. 1804–1815, 2020, doi: 10.1016/j.matpr.2020.03.605.
- [13] L. J. Larminie, James, *Electric Vehicle Technology Explained*, 2nd ed. John Wiley & Sons, Ltd, 2012.
- [14] R. Zhang and L. Gao, "The Brushless DC motor control system Based on neural network fuzzy PID control of power electronics technology," *Optik*, vol. 271, no. August, p. 169879, 2022, doi: 10.1016/j.ijleo.2022.169879.
- [15] T. Wang, H. Wang, H. Hu, X. Lu, and S. Zhao, "An adaptive fuzzy PID controller for speed control of brushless direct current motor," *SN Applied Sciences*, vol. 4, no. 3, 2022, doi: 10.1007/s42452-022-04957-6.
- [16] M. Gheisarnajad, G. Mirzavand, R. R. Ardeshiri, B. Andresen, and M. H. Khooban, "Adaptive Speed Control of Electric Vehicles Based on Multi-Agent Fuzzy Q-Learning," *IEEE Transactions on Emerging Topics in Computational Intelligence*, vol. 7, no. 1, pp. 102–110, 2023, doi: 10.1109/TETCI.2022.3181159.
- [17] B. Naidu Kommula and V. Reddy Kota, "Design of MFA-PSO based fractional order PID controller for effective torque controlled BLDC motor," *Sustainable Energy Technologies and Assessments*, vol. 49, no. February 2021, p. 101644, 2022, doi: 10.1016/j.seta.2021.101644.
- [18] K. H. Tseng, M. Y. Chung, C. Y. Chang, C. L. Hsieh, and Y. K. Tseng, "Parameter optimization of nanosilver colloid prepared by electrical spark discharge method using Ziegler-Nichols method," *Journal of Physics and Chemistry of Solids*, vol. 148, no. April 2020, p. 109650, 2021, doi: 10.1016/j.jpcs.2020.109650.
- [19] Y. Li, Y. Shen, and J. Li, "A Discrete Artificial Bee Colony Algorithm for Stochastic Vehicle Scheduling," *Complex System Modeling and Simulation*, vol. 2, no. 3, pp. 238–252, 2022, doi: 10.23919/CSMS.2022.0012.
- [20] M. He, Z. Wei, X. Wu, and Y. Peng, "An Adaptive Variable Neighborhood Search Ant Colony Algorithm for Vehicle Routing Problem with Soft Time Windows," *IEEE Access*, vol. 9, pp. 21258–21266, 2021, doi: 10.1109/ACCESS.2021.3056067.
- [21] M. Quwaider and Y. Shatnawi, "Neural network model as Internet of Things congestion control using PID controller and immune-hill-climbing algorithm," *Simulation Modelling Practice and Theory*, vol. 101, no. October 2019, p. 102022, 2020, doi: 10.1016/j.simpat.2019.102022.
- [22] M. Awad, A. M. Ibrahim, Z. M. Alaas, A. El-Shahat, and A. I. Omar, "Design and analysis of an efficient photovoltaic energy-powered electric vehicle charging station using perturb and observe MPPT algorithm," *Frontiers in Energy Research*, vol. 10, no. August, 2022, doi: 10.3389/fenrg.2022.969482.
- [23] H. Alrajoubi and S. Oncu, "A Golden Section Search Assisted Incremental Conductance MPPT Control for PV Fed Water Pump," *International Journal of Renewable Energy Research*, vol. 12, no. 3, pp. 1628–1636, 2022, doi: 10.20508/ijrer.v12i3.13119.g8549.
- [24] Z. L. Gaing, "A particle swarm optimization approach for optimum design of PID controller in AVR system," *IEEE Transactions on Energy Conversion*, vol. 19, no. 2, pp. 384–391, 2004, doi: 10.1109/TEC.2003.821821.
- [25] M. Nasri, H. Nezamabadi-Pour, and M. Maghfoori, "A PSO-based optimum design of PID controller for a linear brushless DC motor," *World academy of science, engineering and technology*, vol. 26, no. 40, pp. 211–215, 2007.
- [26] B. Subudhi and R. Pradhan, "Bacterial Foraging Optimization approach to parameter extraction of a photovoltaic module," *IEEE Transactions on Sustainable Energy*, vol. 9, no. 1, pp. 381–389, 2018, doi: 10.1109/TSTE.2017.2736060.
- [27] Z. Li, Y. Qian, H. Wang, X. Zhou, G. Sheng, and X. Jiang, "Partial discharge fault diagnosis based on zernike moment and improved bacterial foraging optimization algorithm," *Electric Power Systems Research*, vol. 207, no. January, 2022, doi: 10.1016/j.epsr.2022.107854.
- [28] I. Journal, M. S. Khande, A. S. Patil, G. C. Andhale, and R. S. Shirsat, "IRJET-Design and Development of Electric scooter Cite this paper Design and Development of Electric scooter," *International Research Journal of Engineering and Technology*, 2020.
- [29] A. Saxena, S. P. Nikam, and B. G. Fernandes, "Study and Design of An Efficient Dual-Motor Powertrain for Two-Wheeled Electric Vehicles," *IECON Proceedings (Industrial Electronics Conference)*, vol. 2019-Octob, pp. 2738–2743, 2019, doi: 10.1109/IECON.2019.8927120.
- [30] Y. Liu *et al.*, "Study on the Design and Speed Ratio Control Strategy of Continuously Variable Transmission for Electric Vehicle," *IEEE Access*, vol. 11, no. September, pp. 107880–107891, 2023, doi: 10.1109/ACCESS.2023.3318323.
- [31] G. Rodrigues Bruzinga, A. J. S. Filho, and A. Pelizari, "Analysis and Design of 3 kW Axial Flux Permanent Magnet Synchronous Motor for Electric Car," *IEEE Latin America Transactions*, vol. 20, no. 5, pp. 855–863, 2022, doi: 10.1109/TLA.2022.9693571.
- [32] A. Upadhyaya and C. Mahanta, "An Overview of Battery Based Electric Vehicle Technologies With Emphasis on Energy Sources, Their Configuration Topologies and Management Strategies," *IEEE Transactions on Intelligent Transportation Systems*, vol. 25, no. 2, pp. 1087–1111, 2024, doi: 10.1109/TITS.2023.3316191.
- [33] W. Zhang, Z. Wang, L. Drugge, and M. Nybacka, "Evaluating Model Predictive Path following and Yaw Stability Controllers for Over-Actuated Autonomous Electric Vehicles," *IEEE Transactions on Vehicular Technology*, vol. 69, no. 11, pp. 12807–12821, 2020, doi: 10.1109/TVT.2020.3030863.
- [34] H. Yue, H. He, and M. Han, "Study on Torsional Vibration Characteristics and Suppression of Electric Vehicles with Dual-motor Drive System," *Journal of the Franklin Institute*, vol. 360, no. 1, pp. 380–402, 2022, doi: 10.1016/j.jfranklin.2022.11.008.
- [35] Gruppo Piaggio, "VESPA ELETTRICA." Accessed: Jan. 18, 2024. [Online]. Available: http://eicma.piaggiogroup.com/mediaObject/events/EICMA_2019/brochure/Vespa/EN-VespaElettrica/original/EN-VespaElettrica.pdf
- [36] G. Shokri and E. Naderi, "Research on simulation and modeling of simple and cost-effective BLDC motor drives," *International Journal of Modelling and Simulation*, vol. 37, no. 1, pp. 15–24, 2017, doi: 10.1080/02286203.2016.1195665.
- [37] B. Singh and R. Kumar, "Simple brushless DC motor drive for solar photovoltaic array fed water pumping system," *IET Power Electronics*, vol. 9, no. 7, pp. 1487–1495, 2016, doi: 10.1049/iet-pel.2015.0852.
- [38] T. Y. Lee, M. K. Seo, Y. J. Kim, and S. Y. Jung, "Motor Design and Characteristics Comparison of Outer-Rotor-Type BLDC Motor and BLAC Motor Based on Numerical Analysis," *IEEE Transactions on Applied Superconductivity*, vol. 26, no. 4, pp. 4–9, 2016, doi: 10.1109/TASC.2016.2548079.
- [39] A. Rajeev Vk and V. Prasad, "Online Adaptive Gain for Passivity-Based Control for Sensorless BLDC Motor Coupled with DC Motor for EV Application," *IEEE Transactions on Power Electronics*, vol. 38, no. 11, pp. 13625–13634, 2023, doi: 10.1109/TPEL.2023.3288939.
- [40] A. Fathima and G. Vijayasree, "Design of BLDC Motor with Torque Ripple Reduction Using Spider-Based Controller for Both Sensorless and Sensorless Approach," *Arabian Journal for Science and Engineering*, no. 0123456789, 2021, doi: 10.1007/s13369-021-05833-y.





- [41] H. Jigang, F. Hui, and W. Jie, "A PI controller optimized with modified differential evolution algorithm for speed control of BLDC motor," *Automatika*, vol. 60, no. 2, pp. 135–148, 2019, doi: 10.1080/00051144.2019.1596014.
- [42] P. Chandran, N. J. Kingston, and N. Muthukrishnan, "Hybrid Controller Design of Bldc Motor For Electric Vehicle Applications," *MysuruCon 2022 - 2022 IEEE 2nd Mysore Sub Section International Conference*, pp. 1–7, 2022, doi: 10.1109/MysuruCon55714.2022.9972716.
- [43] S. Das, A. Biswas, S. Dasgupta, and A. Abraham, "Bacterial foraging optimization algorithm: Theoretical foundations, analysis, and applications," *Studies in Computational Intelligence*, vol. 203, pp. 23–55, 2009, doi: 10.1007/978-3-642-01085-9_2.
- [44] G. Shokri, E. Naderi, and M. Najafpour, "DTC based BLDC Motor Controlled Centrifugal Pump Fed by PI-BFO Tuning Strategy for Buck-Boost Converter in Solar PV Array Water Pumping System," *2019 10th International Power Electronics, Drive Systems and Technologies Conference, PEDSTC 2019*, pp. 769–774, 2019, doi: 10.1109/PEDSTC.2019.8697270.
- [45] M. A. Ibrahim, A. K. Mahmood, and N. S. Sultan, "Optimal PID controller of a brushless DC motor using genetic algorithm," *International Journal of Power Electronics and Drive Systems*, vol. 10, no. 2, pp. 822–830, 2019, doi: 10.11591/ijpeds.v10.i2.pp822-830.
- [46] A. L. Shurajji and S. W. Shneen, "Fuzzy Logic Control and PID Controller for Brushless Permanent Magnetic Direct Current Motor: A Comparative Study," *Journal of Robotics and Control (JRC)*, vol. 3, no. 6, pp. 762–768, 2022, doi: 10.18196/jrc.v3i6.15974.

BIOGRAPHIES OF AUTHORS



Rajnish Kumar     received B.Tech. degree in Electrical Engineering from St. Thomas' College of Engineering and Technology Kolkata, West Bengal, India, in 2016 and M.Tech. degree Control System from NIT Patna, Bihar, India in 2019. He is currently associated with the Department of Electrical Engineering, National Institute of Technology Patna, India, where he is working towards the Ph.D. degree. He can be contacted at email: rajnishk.phd20.ee@nitp.ac.in.



Amitesh Kumar     has done his B.Tech. in Electrical Engineering from Indian Institute of Technology, BHU. He did his Ph.D. in Electrical Engineering from Indian Institute of Technology, Indore. He did his postdoc research at the University of Utah, USA. He has been a research fellow awardee from CSIR, Govt. of India. He is currently working as an assistant professor in Electrical Engineering at National Institute of Technology, Patna. He can be contacted at email: amitesh.ee@nitp.ac.in.